An Integrated Approach for Landslide Susceptibility Mapping Using Remote Sensing and GIS

S. Sarkar and D.P. Kanungo

Abstract

A methodology for landslide susceptibility mapping using an integrated remote sensing and GIS approach is presented. A part of the Darjeeling Himalaya was selected for the model execution. IRS satellite data, topographic maps, field data, and other informative maps were used as inputs to the study. Important terrain factors, contributing to landslide occurrences in the region, were identified and corresponding thematic data layers were generated. These data layers represent the geological, topographical, and hydrological conditions of the terrain. A numerical rating scheme for the factors was developed for spatial data analysis in a GIS. The resulting landslide susceptibility map delineates the area into different zones of four relative susceptibility classes: high, moderate, low, and very low. The susceptibility map was validated by correlating the landslide frequencies of different classes. This has shown a close agreement with the existing field instability condition. The effectiveness of the map was also confirmed by the high statistically significant value of a chi-square test.

Introduction

Landslides are one of the destructive geological processes which cause not only enormous damage to roads, bridges, and houses but also lead to loss of life. Hence, there is a need for landslide susceptibility mapping for identification of potential landslide areas. Landslides are the result of complex interaction among several factors, primarily involving geological, geomorphological, and meteorological factors. The spatial information related to these factors can be derived from remote sensing data, ground based information, and several other data sources. Digital image processing of remote sensing data has a greater degree of objectivity and reproducibility than that obtained by traditional visual interpretation approach. Geographic information systems (GIS) are a very powerful tool for the integration of different types of data. Over the past few years, there have been significant developments of GIS for spatial data analysis. Efficient landslide susceptibility mapping can be carried out by combining GIS with image processing capabilities.

The present study is an attempt towards development of a methodology for landslide susceptibility mapping. This involves the generation of thematic data layers and their spatial analysis within the Darjeeling Himalaya, India. The study also aims to ascertain the utility of remote sensing and GIS.

Trends in Landslide Susceptibility Mapping

In recent years, assessment of landslide susceptibility in the form of hazard zonation has been attempted in a wide variety of environments and using diverse approaches. The different methodologies developed were influenced by the scale of analysis, the availability of input data, and the required details of the hazard map (Brabb, 1984; Nilsen *et al.*, 1979; Varnes, 1984; Wagner *et al.*, 1988; Pachauri and Pant, 1992; Anbalagan, 1992; Sarkar *et al.*, 1995; Mehrotra *et al.*, 1996). These methods are based on the integration of information about the spatial distribution of the factors identified to be important in assessing slope instability. Notable contributions from Carrara (1983) and Chung *et al.* (1995) presented multivariate statistical models for assessing landslide hazards. Other statistical methods, such as the use of information models and fuzzy set theory, were also applied in this context (Yin and Yan, 1988; Juang *et al.*, 1992; Jade and Sarkar, 1993). To evaluate the combined effect of the factors, the use of GIS in the modeling of landslide hazards using many different parameter maps was attempted by several researchers (Carrara *et al.*, 1991; Kingsbury, 1992; Westen, 1994; Nagrajan *et al.*, 1998; Gupta *et al.*, 1999; Dhakal *et al.*, 2000).

Study Area and Geology

The Darjeeling Himalaya, encompassing a total area of 3000 km^2, rises abruptly from the alluvial plains of North Bengal and attains a maximum elevation of about 2600 meters. The area lies between Sikkim on the north, Bhutan towards east, and Nepal towards west. This study focused on Darjeeling hill which lies within latitude 26°56′ to 27°8′ E and longitude 88°10′ to 88°25′ N and covers an area of about 254 km^2 (Figure 1). The area is traversed by many ridges and valleys. The major ridges are at elevations of 2000 m to 2600 m while valleys range in elevation from 500 m to 1000 m. The maximum elevation in the area occurs at Tiger hill at 2584 m. The area is dominated by slopes ranging from 15° to 35° while steep slopes of greater than 35° occupy a much smaller area. In general, gentle slopes of 0° to 15° were found on ridges and at places in regions of lower relief. The main land-use practice in the area is tea plantations. The agriculture lands present are mostly associated with habitation. The area is dominated by thick forests, particularly in the eastern part.

The annual rainfall in the area is on the order of 3000 to 6000 mm. The rainfall pattern is highly seasonal with the majority falling during the monsoon months of June to October. A maximum monthly rainfall of 580 mm was observed in July 2001 at Darjeeling.

Geotechnical Engineering Division, Central Building Research Institute, Roorkee, India (shantanu_cbri@yahoo.com; dpk_cbri@yahoo.com).

Photogrammetric Engineering & Remote Sensing
Vol. 70, No. 5, May 2004, pp. 617–625.

0099-1112/04/7005–0617/$3.00/0

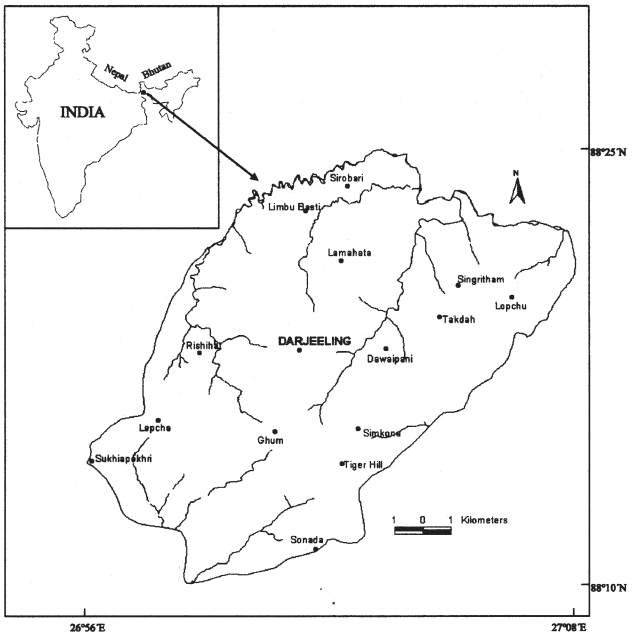

Figure 1. Study area.

The Darjeeling Himalaya lies within the Lesser and Sub Himalayan belt. The tectonic units in the area occur in the reverse order of stratigraphic superposition. In the study area, the Daling group is comprised of low-grade metamorphic rocks, while the Darjeeling Group consists primarily of gneisses. Rocks of the Paro Sub-group, which have characteristics similar to the Darjeeling Group, are present at lower elevations (Acharya and Ray, 1989). The presence of lineaments, hot springs, lakes, water falls, abrupt changes in river gradient, and erraticity in terrace distribution suggested that the area has been undergoing differential uplift along a number of regional and local sub-vertical faults (Banerji *et al.*, 1980).

Data

The data used in this study were IRS-1C LISS III and IRS-1D PAN satellite data (Table 1), topographic maps of the Survey of India (1:25,000 and 1:50,000 scale), and information from published geology and soil maps. The topographic maps and false-color composites (FCCs) of satellite data were used as the base maps for field data collection. Data pertaining to rock types, structural lineaments, slope, soil, land use, and landslides were collected for cross checking and improving the input data layers.

Satellite data were processed using ERDAS Imagine (Version 8.3.1) software. The IRS 1D PAN image was registered with reference to topographic maps by taking input ground control points (GCP) from the PAN image and reference from topographic maps. For the most part, intersections of drainages, roads, and sharp meandering points of rivers were considered as the GCPs. More than 15 GCPs were selected for georeferencing, and resampling was done using the nearest-neighbor interpolation method. During this process, a few GCPs contributing large errors were removed and 11 GCPs with an RMS error of 0.5 were finally considered. The registered PAN image was re-projected from geographic latitude-longitude to the polyconic projection on the modified Everest datum. In a similar way, the LISS-III image was registered to the PAN image with an acceptable RMS error. Verifying feature signatures on both the images ensured the accuracy of the image registration.

The multispectral image was enhanced spatially for better interpretation using an image merging technique (Saraf, 1999). Merging of LISS III and PAN data was undertaken to have the advantage of both a high spatial resolution and a high spectral resolution in a single image. An IHS transformation technique was used, which rescales the grey-scale image (PAN) to the numerical range of the Intensity (I). The hue and saturation components were taken from the LISS III FCC (3:2:1) image. The sensor merge option of the radar module for image enhancement (Erdas Imagine 8.3.1) was used to perform this. This merged image with an enhanced resolution of 5 m showed more clarity and sharpness. The satellite images of the study area are shown in Figure 2.

TABLE 1. ATTRIBUTES OF SATELLITE DATA

Satellite	Sensor	Path/Row	Resolution	Date
IRS 1C	L3	107/52 (50% SAT)	24 m	22 Mar 2000
IRS 1D	PAN	107/52 (10% SAT)	5 m	03 Apr 2000

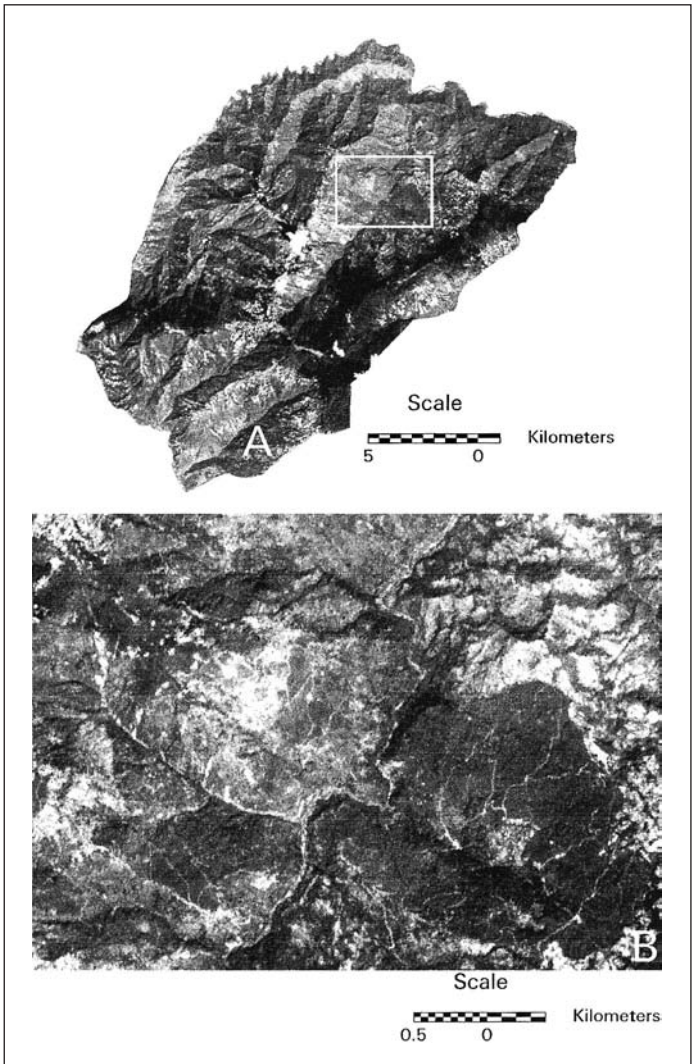

Figure 2. IRS satellite images of the study area. (A) Grey-scale representation of LISS III image (3:2:1). (B) PAN image of the area marked in (A).

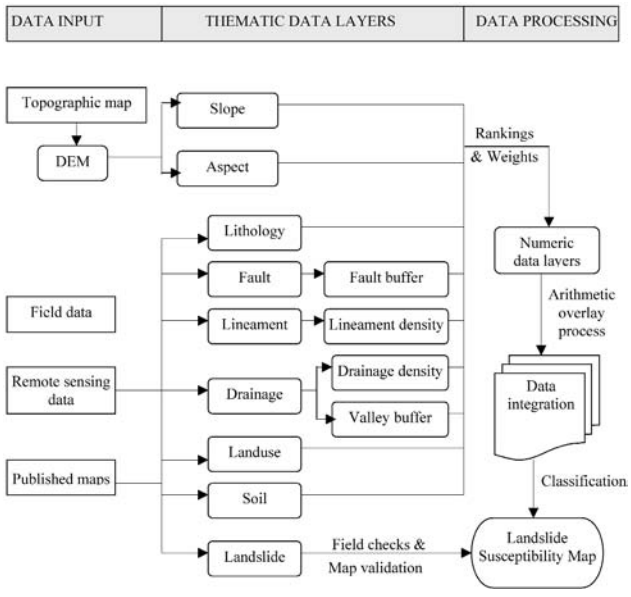

Figure 3. Flow diagram showing the methodology.

Methodology

Because landslides are the result of the interaction of complex factors, the spatial prediction of landslide susceptibility is a difficult task. There are two basic approaches for such a study. One approach is the qualitative map combination where relative weighting values are assigned to the factors and their classes on the basis of field knowledge and experience. The other approach uses statistics to compute the weighting values based on the relationship of the factors with existing landslides. However, if the data set is small and sufficient landslide information is not available, the statistical approach may give erroneous results. In our study we have adopted a technique of qualitative map combination by developing a rating system, which is based on the relative importance of factors influencing slope instability in the study area.

Because, for each land system, a different model is required which must reflect the specific operating conditions (Carrara, 1991), the technique adopted here may be applicable only to this part of the Himalaya having geology, geomorphology, and land-use practices different from other parts of the Himalaya. The methodology involved selection of factors, generation of data layers in the GIS, numerical rating assignment to factors, data integration in the GIS, computation of the landslide potential index, suitable classification of landslide susceptibility, and validation of the resulting map. An attempt was also made to validate the map with existing landslide distribution and a statistical significance test. These steps are shown in a flow diagram (Figure 3).

Thematic Data Layers

Selection of factors and preparation of corresponding thematic data layers are crucial components of any model for landslide susceptibility mapping. The factors governing instability in a terrain are primarily geology, slope morphology, drainage, land use, anthropogenic activity, seismicity, and climatic condition. These factors can be broadly grouped into two categories—the preparatory factors which make the slope susceptible to movement and the triggering factors which set off the movement (Crozier, 1986). The triggering factors such as rainfall and earthquakes, whose magnitude and temporal behavior are difficult to gauge, could not be considered here due to non-availability of past records regarding landslide occurrence. The factors considered in our study are essentially the preparatory factors for which pertinent data can be collected from available resources as well as from the field. These were slope, aspect, lithology, soil type, drainage density, lineament density, presence of faults, land use, and presence of valleys. The selection of these factors and their classes was primarily based on the field observations of existing landslides and their associated terrain factors. Based on the information collected from available maps, satellite data, and field investigations, thematic data layers were generated. A landslide distribution map was also prepared. The mapping was done at a scale of 1:25,000. The details of these layers are described in the following paragraphs.

Digital Elevation Model and Its Derivatives

A digital elevation model (DEM) can be used to derive information on elevation, slope aspect, slope angle, watersheds, and cut and fill volumes. Survey of India topographic map sheets of the Darjeeling area at 1:25,000 and 1:50,000 scales (1972 and 1987) were employed for generating the DEM. Contours at 10-m and 20-m intervals were considered for generating the DEM using the TIN module of Arc View 3D Analyst (Figure 4).

Slope angle is one of the key factors in inducing slope instability. A slope map with a 25-m grid cell size was generated from the DEM. The map represents the spatial distribution of slope values in the area. These were classified into five classes with a 10° interval as per the slope classification of earlier workers (Anbalagan, 1992; Dhakal *et al.*, 2000). The maximum area was occupied by the 15° to 25° and 25° to 35° slope classes, while steep slopes greater than 35° are much less frequent in the area. A slope aspect map with a 25-m grid cell size was also generated from the DEM.

Lithology

The lithology map was derived from the geological map (scale 1:250,000) of the Sikkim-Darjeeling area (Acharya and Ray, 1989) which was scaled to 1:25,000 for field investigation. Necessary modifications were incorporated after field

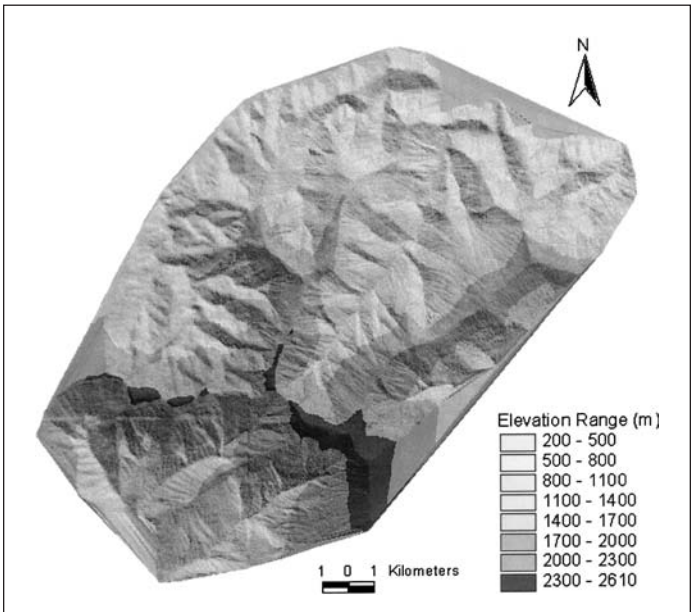

Figure 4. Digital Elevation Model of the study area.

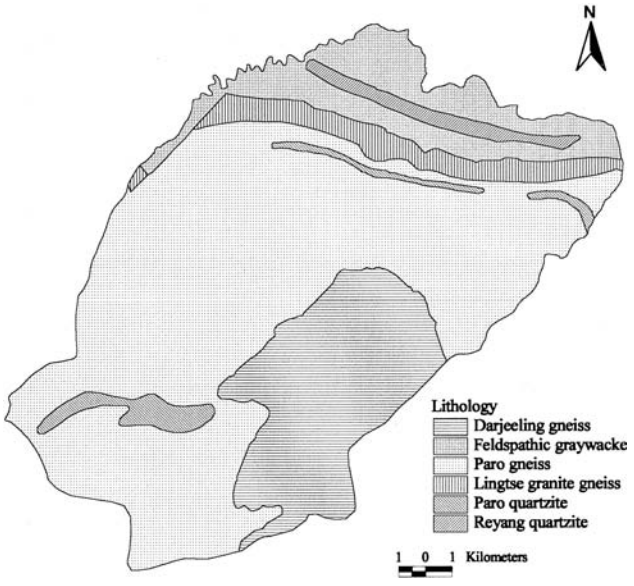

Figure 5. Lithology map.

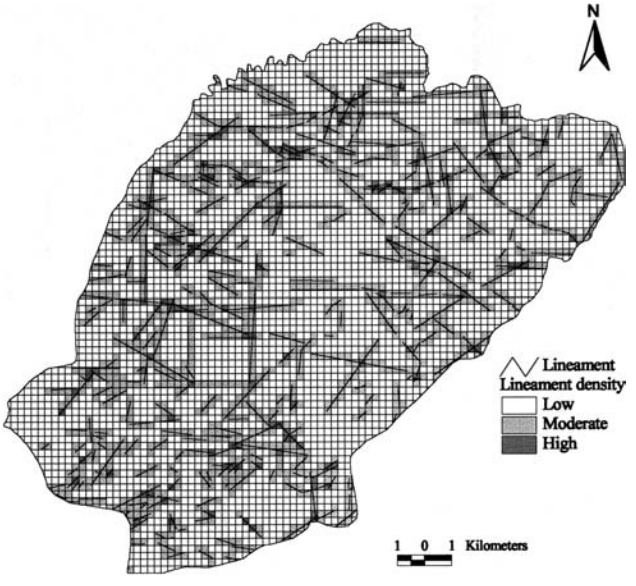

Figure 6. Lineament density map.

verification in order to prepare the lithology map (Figure 5). There are six rock types present in the area. These are Darjeeling gneiss, Paro gneiss, Lingtse granite gneiss, feldspathic greywacke, and quartzites of the Paro sub-group and the Reyang group. The Lingtse granite gneiss are strongly foliated and sheared, showing very high weathering at most locations. The Paro gneisses are stronger and coarse grained than are the Darjeeling gneiss of higher metamorphic grade. The quartzites are stronger than the other rocks in the area. However, all the rocks are folded, faulted, and sheared to varying degrees, and they have been subjected to high levels of weathering along the drainage channels.

Faults and Lineaments

The lineaments showing fractures, discontinuities, and shear zones were interpreted from the LISS III and merged images. The lineament density for each 250- by 250-m cell was computed using the line density analyst extension (Saraf, 2000) of Arc View GIS and were classified into low (0), moderate (0 to 0.005 m/m^2), and high (0.005 to 0.013 m/m^2) density. The lineaments were superimposed on the lineament density map (Figure 6). The map shows no lineaments in the low density class, a single lineament in the moderate class, and mostly more than one and/or intersecting lineaments in the high density class. Further faults, which are mega lineaments, showing offsets of ridges and drainage lines, were also identified. These were verified at a few locations in the field showing considerable indications of shearing and faulting.

Drainage

The drainage map was prepared from the topographic maps with additional inputs from the satellite images. The drainage density was computed considering a 250- by 250-m cell and classified with equal intervals into low (0 to 0.006 m/m^2), moderate (0.006 to 0.012 m/m^2), and high (0.012 to 0.0185 m/m^2) density. The drainages superimposed on the drainage density map (Figure 7) show relatively more numbers and closely spaced drainage channels in the high density class than in the moderate and low classes.

Soil

The topsoil cover on a slope has an influence on landslide occurrence as observed in the field. For our study, the soil map was derived from a regional soil map at a 1:250,000 scale (NBSSLUP, 1990). The soils present in the area are coarse loamy, fine loamy, and loamy skeletal. The soil map was field checked at a few locations. The random soil samples were studied in the laboratory to investigate the variation in grain size. The study supported the soil classification as shown on the map (Figure 8).

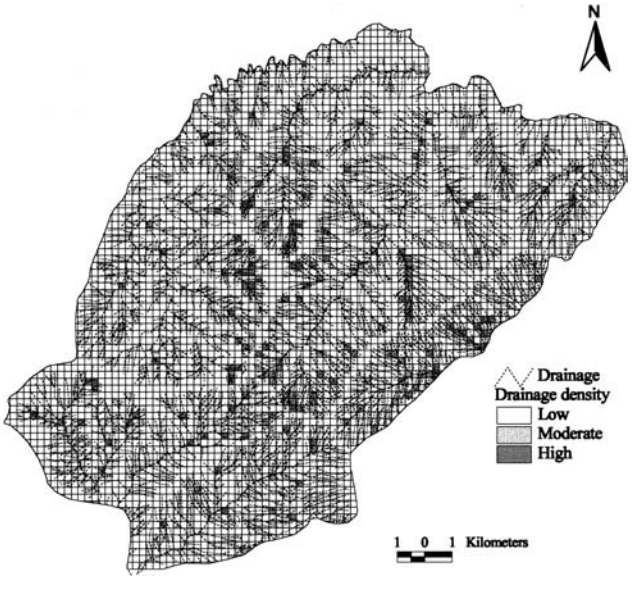

Figure 7. Drainage density map.

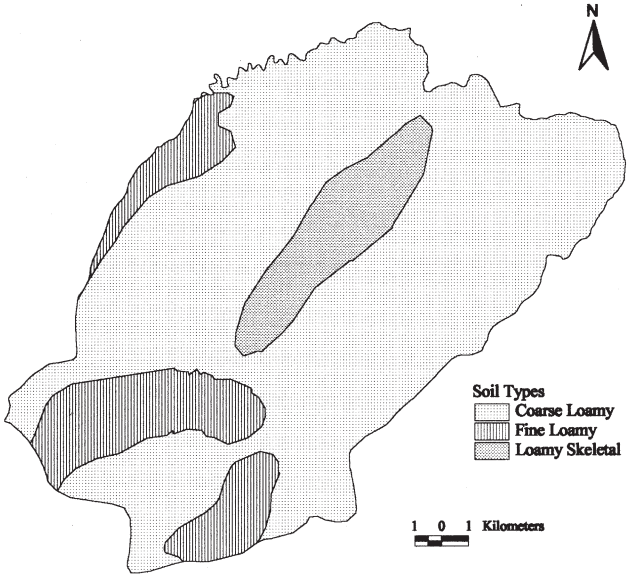

Figure 8. Soil map.

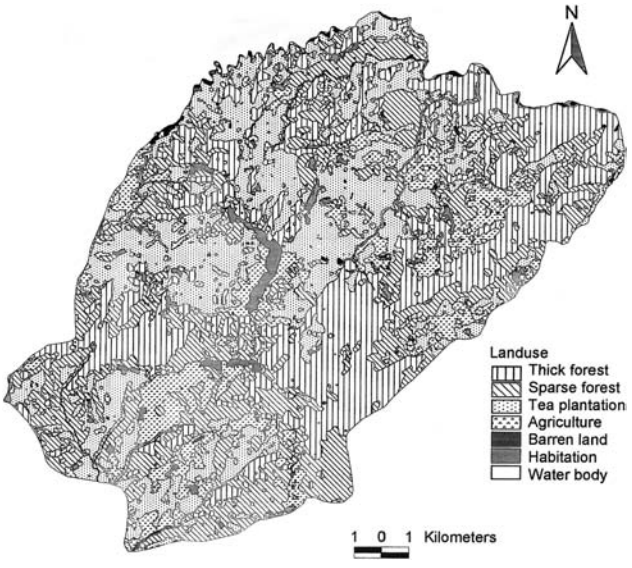

Figure 9. Land-use map.

Land Use

A land-use map in hilly areas in general shows the distribution of forest cover, water bodies, and types of land-use practices. To prepare this map, LISS III and merged images were processed in Erdas Imagine software using unsupervised and supervised classification techniques. An unsupervised classification is the natural grouping of pixels in the input image data. While performing the unsupervised classification, the output was generated for 20 classes. These classes were compared with different land-use types of the area based on the data from field and topographic map sheets. It was observed that the areas covered by thick forest, sparse forest, barren land, and water bodies were correctly classified. These classes were considered as training samples for the supervised classification process. The ground truth for other land-use classes present in the area (agricultural land, tea plantations, and habitation) was collected from the field and identified on the image by defining polygons. Finally, the land-use map was prepared using the supervised classification technique with the maximum-likelihood parametric rule. After preparing the map, it was again checked in the field. Some errors were observed, particularly in the areas of tea plantations and agricultural land. These errors were mapped in the field and subsequently rectified in the data layer. The land-use map was finally transferred to the GIS (Figure 9).

Landslide Distribution

The important aspects for detecting landslides in satellite imagery are spectral characteristics, size, shape, contrast, and morphological expression. Interpretability is influenced by the contrast that results from the spectral difference between the landslide and its surroundings. High-resolution satellite images such as SPOT PAN of 10-m resolution and ATM imagery of 7.5-m resolution were used by Mason *et al.* (1998) for landslide detection.

In this study, PAN, and PAN-LISS III merged images were used for landslide detection. Because the landslides were mostly bare of vegetation, they showed high reflectance. They were found to be mostly circular to elliptical in shape. A few of the landslides mapped were cross-checked in the field and the map was modified accordingly. A majority of the landslides observed were debris slides. However, in some cases rotational and complex types of failures were also present. A few rock falls of small magnitude were also identified in the field. Some of the main contributing factors for landslides, as observed in the field, were excessive water flow along the drainage channels, particularly during the rains, and steep slopes and weathered disintegrated rocks in the vicinity of faults/structural lineaments. The landslide map contains 101 landslides showing the areas occupied by sliding activity. It includes source area and debris cover (Figure 10). The majority of landslides have aereal extents of 500 m^2 to 2000 m^2.

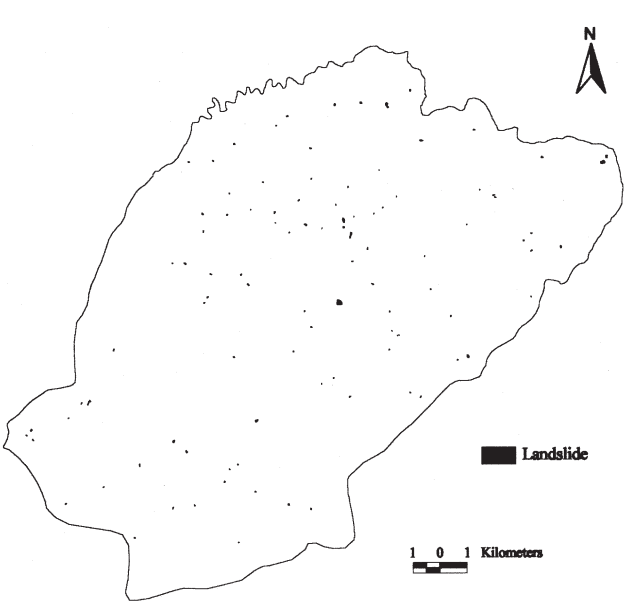

Figure 10. Landslide distribution map.

The landslide density in the study area is 0.39 per km^2. Landslides are distributed over the entire area; however, maximum clustering was observed in the northwestern part.

Numerical Rating Scheme

The identification of potential landslide areas requires that the factors considered be combined in accordance with their relative importance to landslide occurrence. This can be achieved by developing a rating scheme in which the factors and their classes are assigned numerical values. A rating scheme was developed based on the associated causative factors for landslides surveyed in the field and on the knowledge from previous work. In this scheme, the factors were assigned a numerical ranking on a 1 to 9 scale in order of importance. Weights were also assigned to the classes of the factors on 0 to 9 ordinal scale where higher weight indicates more influence towards landslide occurrence. The scheme was suitably modified by undertaking several iterations using different combinations of weights. The rating scheme given in Table 2 is described below.

TABLE 2. RANKS AND WEIGHTS FOR FACTORS AND THEIR CLASSES

Data Layers	Classes	Ranks	Weights
Drainage density	1. Low	9	1
	2. Moderate		5
	3. High		9
Lineament density	1. Low	8	0
	2. Moderate		5
	3. High		9
Slope	1. 0°−15°	7	1
	2. 15°−25°		3
	3. 25°−35°		5
	4. 35°−45°		7
	5. >45°		9
Lithology	1. Reyang Quartzite	6	1
	2. Paro Quartzite		1
	3. Feldspathic Greywacke		3
	4. Paro Gneiss		5
	5. Darjeeling Gneiss		7
	6. Lingtse Granite Gneiss		9
Fault buffer	1. 0–250 m	5	9
	2. 250–500 m		6
	3. 500–750 m		3
	4. >750 m		0
Land use	1. Water body	4	0
	2. Thick forest		1
	3. Built-up area		2
	4. Tea plantation		3
	5. Agriculture land		5
	6. Sparse forest		7
	7. Barren land		9
Valley buffer	1. 0–100 m	3	6
	2. >100 m		0
Soil	1. Fine loamy	2	3
	2. Coarse loamy		6
	3. Loamy skeletal		9
Aspect	1. Flat	1	0
	2. North		1
	3. Northeast		4
	4. East		7
	5. Southeast		8
	6. South		9
	7. Southwest		6
	8. West		3
	9. Northwest		2

In the study area, it was observed that most of the landslides were associated with drainage channels; hence, the maximum weight was assigned to high drainage density. The next important factor considered was lineament density. Here, the maximum weight was given to the high lineament density because the highly fractured and jointed formation showed more potential to landslides. Because steeper slopes are more prone to landslides, the slope classes were given weights in descending order. The competent rocks such as quartzite and greywacke are less susceptible to landslides than are the gneisses; hence, the weights for lithology were assigned accordingly after field observations. The presence of a fault in an area indicates a weak zone due to the presence of weathered and shattered rock masses. To account for the influence of fault zones, a fault buffer of 250 m was considered because of signs of instability observed along the faults within this range. Occurrence of landslides depends much on the type of land use. Barren slopes are more susceptible to erosion as compared to areas with thick forests; hence, a maximum weight was assigned to barren slopes and a minimum weight was assigned to thick forests. Based on the field observation, the weights for other land-use classes fell between these two. It was observed in the field that at a few locations the erosion activity and toe cutting along major streams had influenced slope instability. Hence, a valley buffer of 100 m, considering the major streams (4th and higher order drainages), was accounted because the erosional activities were observed within this range. Coarse grained and less cohesive soils are more prone to erosion. Hence, weights were assigned to soil classes on the basis of soil types present in the area. Slope aspect has an indirect influence on slope instability. In general, south-facing slopes have a lesser vegetation density as compared to north-facing slopes; hence, erosional activity is relatively greater in the former case (Sinha *et al.*, 1975). Based upon the landslide distribution, south- and east-facing slopes were considered to have more potential for landslides (Dhakal *et al.*, 2000). Considering these facts and field observation, slope aspect classes were given weights accordingly.

Data Integration and Landslide Susceptibility Mapping

The numerical data layers representing weight values of the factor classes as attribute information were generated from the thematic data layers for data integration and spatial analysis in the GIS. The input data layers were multiplied by their corresponding ranks and were added up to obtain the Landslide Potential Index (LPI) for each 25- by 25-m cell: i.e.,

$$\text{LPI} = \sum_{i=1}^{9} (R_i \times W_{ij}) \quad (1)$$

where R_i denotes the rank for factor i and W_{ij} denotes the weight of class j of factor i.

The arithmetic overlay approach built into Arc View Model Builder was adopted for this. Such an arithmetic overlay process accepts both continuous and discrete grid layers, and the derived data are continuous grid data layer.

The landslide potential index obtained ranged from 39 to 323. These could be classified into several landslide susceptible classes. A judicious way for such classification is to search for abrupt changes in values (Davis, 1986). For this purpose, a graph showing LPI frequency was prepared which showed many oscillations. Hence, moving averages with averaging window lengths of 3, 7, and 11 were considered for smoothing the curve to produce a better classification. The window length 3 means that the frequency value in the corresponding graph at any point is an average of the three consecutive values centered at that point. The class boundaries were drawn at significant changes in gradients of the graph supplemented

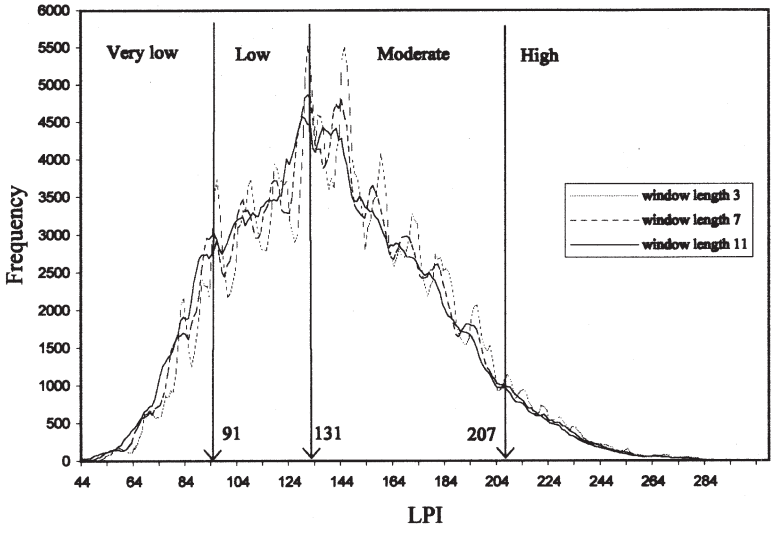

Figure 11. Frequency distribution of landslide potential index.

by a field check (Figure 11). The area was classified into high, moderate, low, and very low landslide susceptibility (Table 3). The landslide susceptibility map, which delineates the relative potential zones for landslide occurrence, is shown in Figure 12.

TABLE 3. LANDSLIDE POTENTIAL INDEX (LPI) AND SUSCEPTIBILITY CLASSES

Susceptibility Class	LPI
Very low	39–91
Low	92–131
Moderate	132–207
High	208–323

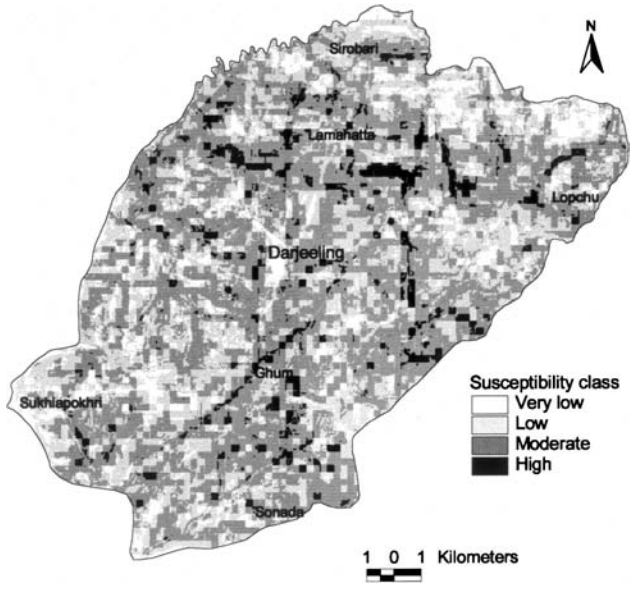

Figure 12. Landslide susceptibility map.

Map Validation

The landslide susceptibility map thus prepared was checked in the field, and it was observed that the areas of high susceptible zones showed significant indications of slope instability marked by landslides, erosion, and subsidence. However, to assess the quality of the landslide susceptibility map, it is important to compute the landslide frequency of each class (Sarkar, 1996). Landslide frequency, i.e., the number of landslides per square kilometer for each class, was computed as given in the Table 4. The frequencies for very low, low, and moderate susceptibility classes are 0, 0.16, and 0.49 per km^2, respectively, while the frequency for the high susceptibility class is significantly higher (1.78 per km^2). This shows a gradual increase in landslide frequency values from the very low to the highly susceptible class. There is also a considerable separation of frequency values in-between the classes. Hence, it can be inferred that the landslide susceptibility zones reflect the existing field instability conditions. The areas in high susceptible zones that are devoid of landslides indicate potential landslide zones.

Further, to see the effectiveness of the susceptibility map, a statistical significance chi-square test was performed. For the null hypothesis, it was assumed that the number of landslide cells present in the susceptibility classes was purely due to chance. The observed cells with and without landslides for each of the four classes were determined from the map, and the expected cells for the same were estimated from the observed values (Table 5). The chi-square value computed for the above data is 165.69 with a probability of 1.08031E − 35. The standard chi-square value with three degrees of freedom at the 0.01 significance level is 11.3. Thus, the null hypothesis

TABLE 4. DISTRIBUTION OF SUSCEPTIBILITY CLASSES AND LANDSLIDES

Susceptibility Class	Area (km^2)	Number of Landslide	Frequency (/km^2)
Very low	27.006	0	0
Low	86.084	14	0.163
Moderate	128.509	64	0.498
High	12.859	23	1.789

TABLE 5. OBSERVED AND EXPECTED RESULTS FOR THE CHI-SQUARE TEST

	Observed					Expected				
	Very Low	Low	Moderate	High	Total	Very Low	Low	Moderate	High	Total
Cells without landslide	43205	137686	205389	20521	406801	43173.76	137622.68	205446.33	20558.22	406801
Cells with landslide	4	49	225	54	332	35.235	112.317	167.67	16.778	332
Total	43209	137735	205614	20575	407133	43209	137735	205614	20575	407133

could be rejected and the susceptibility map could be considered as statistically significant.

Conclusions

The methodology for landslide susceptibility mapping presented here involves the generation of thematic data layers, development of a suitable numerical rating scheme, spatial data integration, and validation of results. In the present study, remote sensing and GIS were extensively used. The merging of multispectral and panchromatic satellite data greatly improved the quality of terrain features in the image. Application of GIS was found immensely useful for thematic data layer generation and for their spatial data analysis, which involved complex operations.

The numerical rating scheme of the methodology was improved iteratively by evaluating and optimizing the results. However, because the landslide contributing factors vary from region to region, this rating scheme may not be suitable in other parts of the Himalaya. The landslide susceptibility map divides the area into different zones corresponding to four relative susceptibility classes. The result was validated on the basis of landslide distribution in the area. The statistically significant value of the chi-square test also validates the susceptibility classes of the map. Hence, it may be inferred that the map correlates well with existing field conditions. However, the quality of the susceptibility map can be further improved by incorporating more factors. Further, any change in the natural environment by human interference, such as implementation of development projects, deforestation, etc., may change the existing landslide susceptibility of the area. Hence, such maps should be updated periodically.

The landslide susceptibility maps help in decision making, while implementing a development project in the terrain. It is always better to avoid the highly susceptible zones but, if not possible, corrective measures must be worked out to minimize the probability of landslide occurrences.

Acknowledgments

The authors are grateful to the Director, CBRI, for his kind permission to publish this work. The authors thank Prof. P.K. Gupta and Prof. V.N. Singh, IIT, Roorkee, for their valuable suggestions in improving the manuscript. The comments of the reviewers greatly improved the quality of the paper. Financial support from the Ministry of Environment & Forests, New Delhi, is also acknowledged.

References

Acharya, S.K., and K.K. Ray, 1989. *Daling Group and Related Rocks*, Special Publication No. 22, Geological Survey of India, Calcutta, India, 105 p.

Anabalagan, R., 1992. Landslide hazard evaluation and zonation mapping in mountainous terrain, *Engineering Geology*, 32:269–277.

Banerji, P.K., P.K. Guha, and L.C. Dhiman, 1980. Inverted metamorphism in the Sikkim-Darjeeling Himalaya, *Geological Society of India*, 21:330–342.

Brabb, E.E., 1984. Innovative approaches to landslide hazard and risk mapping, *Proceedings of the 4th International Symposium on Landslides*, 16–21 September, Toronto, Ontario, Canada (Canadian Geotechnical Society, Toronto, Ontario, Canada), 1:307–324.

Carrara, A., 1983. Multivariate models for landslide hazard evaluation, *Mathematical Geology*, 15(3):403–427.

Carrara, A., M. Cardinali, F. Detti, F. Guzzetti, V. Pasqui, and P. Reichenbach, 1991. GIS techniques and statistical models in evaluating landslide hazard, *Earth Surface Processes and Landforms*, 16(5):427–445.

Chung, C.F., A.G. Fabbri, and C.J. van Westen, 1995. Multivariate regression analysis for landslide hazard zonation, *Geographical Information Systems in Assessing Natural Hazards* (A. Carrara, and F. Guzzetti, editors), Kluwer Academic Publishers, Dordrecht, The Netherlands, pp. 107–134.

Crozier, M.J., 1986. *Landslides: Causes, Consequences and Environment*, Croom Helm Australia Pty. Ltd., London, United Kingdom, 252 p.

Davis, J.C., 1986. *Statistics and Data Analysis in Geology*, John Wiley & Sons, New York, N.Y., 646 p.

Dhakal, A.S., T. Amada, and M. Aniya, 2000. Landslide hazard mapping and its evaluation using GIS: An investigation of sampling schemes for a grid-cell based quantitative method, *Photogrammetric Engineering & Remote Sensing*, 66(8):981–989.

Gupta, R.P., A.K. Saha, M.K. Arora, and A. Kumar, 1999. Landslide hazard zonation in a part of the Bhagirathi valley, Garhwal Himalayas, using integrated remote sensing-GIS, *Himalayan Geology*, 20(2):71–85.

Jade, S., and S. Sarkar, 1993. Statistical model for slope instability classifications, *Engineering Geology*, 36:71–98.

Juang, C.H., D.H. Lee, and C. Sheu, 1992. Mapping slope failure potential using fuzzy sets, *Geotechnical Engineering*, 118 (3):475–494.

Kingsbury, P.A., W.J. Hastie, and A.J. Harrington, 1992. Regional landslip hazard assessment using a GIS, *Proceedings of the 6th International Symposium on Landslides*, 10–14 February, Christchurch, New Zealand (A.A. Balkema, Rotterdam, The Netherlands), 2:995–1000.

Mason, P.J., M.S. Rosenbaum, and J.M. Moore, 1998. Digital image texture analysis for landslide hazard mapping, *Geohazards in Engineering Geology* (J.G. Maund and M. Eddleston, editors), Engineering Geology Special Publications, Geological Society, London, 15:297–305.

Mehrotra, G.S., S. Sarkar, D.P. Kanungo, and K. Mahadevaiah, 1996. Terrain analysis and spatial assessment of landslide hazards in parts of Sikkim Himalaya, *Geological Society of India*, 47:491–498.

Nagarajan, R., A. Mukherjee, A. Roy, and M.V. Khire, 1998. Temporal remote sensing data and GIS application in landslide hazard zonation of part of Western ghat, India, *Remote Sensing*, 19:573–585.

NBSSLUP, 1990. *Soil and Land Resources Atlas—West Bengal*, National Bureau of Soil Survey and Land Use Planning (ICAR), Nagpur, India.

Nilsen, T.H., R.H. Wright, T.C. Vlasic, and W. Spangle, 1979. *Relative Slope Stability and Landuse Planning in the San Francisco Bay Region, California*, U.S. Geological Survey Professional Paper 944, U.S. Government Printing Office, Washington, D.C., 96 p.

Pachauri, A.K., and M. Pant, 1992. Landslide hazard mapping based on geological attributes, *Engineering Geology*, 32:81–100.

Saraf, A.K., 1999. IRS-1C-LISS-III and PAN data fusion: An approach to improve remote sensing based mapping techniques, *International Journal of Remote Sensing*, 20(10):1929–1934.

_____, 2000. DLR density analyst extension (ver. 1.0) for Arc View GIS 3.2, Environmental Systems Research Institute, Inc., Redlands, California, URL: http://www.esri.com.

Sarkar, S., 1996. *Landslide Hazard Zonation and Slope Stability Assessment Techniques: Applications to Srinagar-Rudraprayag, Garhwal Himalaya*, Unpublished Ph.D. Thesis, University of Roorkee, Roorkee, India, 156 p.

Sarkar, S., D.P. Kanungo, and G.S. Mehrotra, 1995. Landslide hazard zonation: A case study in Garhwal Himalaya, India, *Mountain Research and Development*, 15(4):301–309.

Sinha, B.N., R.S. Varma, and D.K. Paul, 1975. *Landslides in Darjeeling District (West Bengal) and Adjacent Areas*, Bulletins of the Geological Survey of India, Series B, No. 36, Calcutta, India, 45 p.

van Westen, C.J., 1994. GIS in landslide hazard zonation: A review, with examples from the Andes of Colombia, *Mountain Environments and Geographical Information Systems* (M.F. Price and D.I. Heywood, editors), Taylor & Francis Publishers, London, United Kingdom, pp. 135–165.

Varnes, D.J., 1984. *Landslide Hazard Zonation: A Review of Principles and Practice*, Natural Hazards 3, Commission on Landslides of the IAEG, UNESCO, Paris, France, 63 p.

Wagner, A., E. Leite, and R. Olivier, 1988. Rock and debris slides risk mapping in Nepal—A user friendly PC system for risk mapping, *Proceedings of the 5th International Symposium on Landslides*, 10–15 July, Lausanne, Switzerland (A.A. Balkema, Rotterdam, The Netherlands), 2:1251–1258.

Yin, K.I., and T.Z. Yan, 1988. Statistical prediction models for slope instability of metamorphosed rocks, *Proceedings of the 5th International Symposium on Landslides*, 10–15 July, Lausanne, Switzerland (A.A. Balkema, Rotterdam, The Netherlands), 2:1269–1272.

(Received 13 September 2002; revised and accepted 16 April 2003; revised 03 June 2003)